A lake-level chronology based on feldspar luminescence dating of beach ridges at Tangra Yum Co (southern Tibet)

CrossMark

Eike F. Rades [a,b,*], Sumiko Tsukamoto [b], Manfred Frechen [b], Qiang Xu [c], Lin Ding [c]

[a] Institut für Geologie und Paläontologie, Westfälische Wilhelms-Universität Münster, Corrensstraße 24, 48149 Münster, Germany
[b] Leibniz Institute for Applied Geophysics (LIAG), Geochronology & Isotope Hydrology, Stilleweg 2, 30655 Hannover, Germany
[c] Institute of Tibetan Plateau Research, Chinese Academy of Sciences, 4A Datun Road, Chaoyang District, Beijing 100101, China

ABSTRACT

Many lakes on the Tibetan Plateau exhibit strandplains with a series of beach ridges extending high above the current lake levels. These beach ridges mark former lake highstands and therefore dating their formation allows the reconstruction of lake-level histories and environmental changes. In this study, we establish a lake-level chronology of Tangra Yum Co (fifth largest lake on the Tibetan Plateau) based on luminescence dating of feldspar from 17 beach-ridge samples. The samples were collected from two strandplains southeast and north of the lake and range in elevation from the current shore to 140 m above the present lake. Using a modified post-infrared IRSL protocol at 170°C we successfully minimised the anomalous fading in the feldspar IRSL signal, and obtained reliable dating results. The luminescence ages indicate three different stages of lake-level decline during the Holocene: (1) a phase of rapid decline (~50 m) from ~6.4 to ~4.5 ka, (2) a period of slow decline between ~4.5 and ~2.0 ka (~20 m), and (3) a fast decline by 70 m between ~2 ka and today. Our findings suggest a link between a decrease in monsoonal activity and lake-level decline since the early Holocene.

© 2015 University of Washington. Published by Elsevier Inc. All rights reserved.

Introduction

Changes in water level are well known indicators for various geological and climatological processes. These changes can be understood using geological markers such as wave-built beach ridges, which form at or near to the current shoreline (Otvos, 2000). Large successions of beach ridges known as beach ridge plains or strandplains can be found all over the world (Ortlieb et al., 1992; Anthony, 1995; Harvey, 2006; Forsyth et al., 2010). Comprising the former shorelines, they are suited to reconstruct past sea or lake-level changes. Dating of beach ridges is often conducted using luminescence dating especially where ^{14}C is not reliable or samples are not available (Jacobs, 2008). Luminescence dating studies on beach ridges have been carried out at various sites and different settings (Nielsen et al., 2006; Tamura et al., 2012; Hipondoka et al., 2014). Unless related to tectonics, these changes can often be correlated to changes in environmental conditions or climatic events.

The past climate conditions on the Tibetan Plateau, particularly for the time period after the Last Glacial Maximum (LGM), have been the focus of researchers (e.g. Gasse et al., 1991; Wei and Gasse, 1999; Wang et al., 2002; Morrill et al., 2006; Daut et al., 2010; Frenzel et al., 2010; Mischke et al., 2010; Opitz et al., 2012; Doberschütz et al., 2013). A large part of these efforts focused on more than 800 lakes with a size of >1 km[2] covering the plateau (Ma et al., 2011). Most of these lakes are surrounded by distinctive shorelines indicating higher lake levels during the geological past. The timing of the lake-level fluctuations and their relation to climatic processes has been discussed in several studies (e.g. Sun et al., 2010; Zhao et al., 2011; Liu et al., 2013; Lai et al., 2014; Yan and Wünnemann, 2014), but a detailed reconstruction of the lake-level variations is still missing for most of the Tibetan lakes. Luminescence dating studies have been carried out on major lakes of the Tibetan Plateau to reconstruct the lake-level chronologies. Liu et al. (2011) successfully tested various sediments from different sources at lake Qinghai for their luminescence dating suitability. Other studies using luminescence dating on beach ridges and lake sediments tried to establish lake levels for definite points in time to correlate with proxies from lake sediments (Liu et al., 2011). Furthermore, other studies intended to set up a reliable chronological framework for lake level fluctuations and to correlate to global chronologies such as the marine oxygen isotope records (Li et al., 2009) or the variance of the monsoonal forcing on the Tibetan Plateau (Chen et al., 2013). However, most of these they lack a complete lake-level record to be able to reconstruct long time lake-level history.

Tangra Yum Co, a major lake in a closed basin on the Tibetan Plateau (Fig. 1), exhibits strandplains with large successions of beach ridges. In this study we present a detailed lake-level chronology of Tangra Yum

* Corresponding author at: Currently working at Institute for Applied Geology, University of Natural Resources and Life, Sciences, Peter Jordan-Str. 70, 1190 Vienna, Austria.
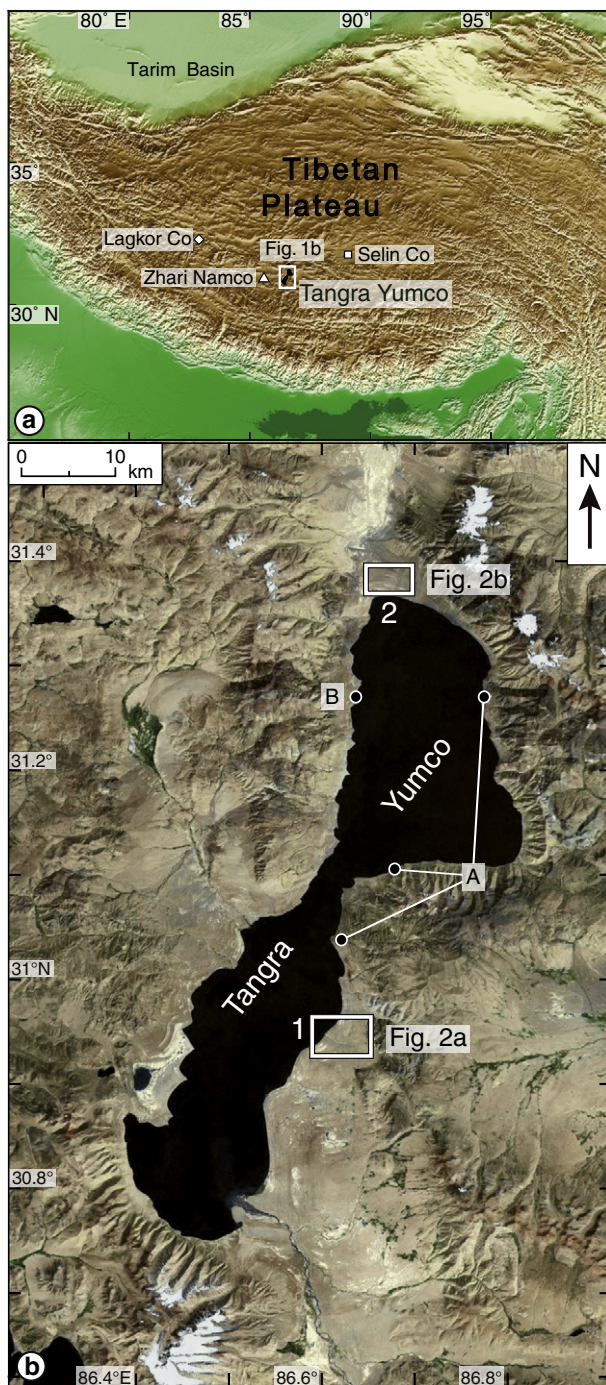E-mail address: EikeF.Rades@gmail.com (E.F. Rades).

Figure 1. (a) Digital elevation model of the Tibetan Plateau showing the location of Tangra Yum Co and the lakes discussed in Lake level and monsoonal activity. The white rectangle marks the outline of Figure 1b. (b) Satellite image of Tangra Yum Co giving an overview of the lake. The white rectangles indicate the locations of the two profiles of beach ridges (see Figs. 2a, b). The locations of the sampling sites of the studies of Rades et al. (2013)(A) and Long et al. (2012) (B) discussed in Lake level and monsoonal activity are given by black circles on the eastern and northwestern shore.

Co dating successive beach-ridge samples from two strand plains using feldspar luminescence dating. Feldspar luminescence dating has shown promising results on a bore core of Tangra Yum Co compared to radio-carbon ages (Long et al., 2015). Using a post-IR IRSL protocol (pIRIR) with an elevated temperature of 170°C we successfully minimised the anomalous fading rates. This study is a part of an ongoing Sino–German research cooperation (http://www.tip.uni-tuebingen.de/index.php/en/) in which Tangra Yum Co is one of the prime targets for paleo-

climatological investigations. This study aims to establish a detailed and reliable lake-level chronology with numerical dating to enable correlations with similar studies and climatic events on the Tibetan Plateau or worldwide.

Geological setting and sampling

Geomorphology around Tangra Yum Co

Tangra Yum Co is located in a north–south trending graben system in southern Tibet. With a surface of 835 km^2 it is one of the largest lakes on the Tibetan Plateau (Shao et al., 2008). Furthermore, it exhibits morphologically well developed strath terraces up to 180 m above the current lake level in the more erosional areas and beach-ridge se-quences of more than 220 m above the current lake level in areas with a more depositional regime. This implies the largest lake-level varia-tions on the whole plateau. The lake has a conspicuous shape, which can be ascribed to two larger basins which are connected by a "bottle-neck" in the middle of the lake.

At the western and southern shore two major rivers drain into the Tangra Yum Co (Fig. 1), also numerous small streams flow into the lake at various locations. Due to the incoming river sediments at these locations the shoreline is dominated by a depositional regime. At the northern and southeastern shore large strandplains have formed exhibiting successions of beach ridges. Especially at the northern shore the beach ridges extend to their highest elevation of more than 220 m above current lake level. The beach ridges can be found in various sizes but are mostly around 10–25 m wide and up to ~10 km long. The height differs between a few decimetres and 2–3 m. The rest of the lake surroundings are only scarcely covered by sediments and the lake formed strath terraces during distinct phases of its decline. At the north-eastern shore some beach ridges were found on terraces but they seem to be very rare and bound to the sediment inflow of the small rivers near to these sites. Which therefore are the only locations where lake sedi-ments can be found, because the incised river valleys were filled during the lake highstands.

Beach-ridge sediments indicating precise paleo-lake levels like the ones that can be found at Tangra Yum Co are exceptional. The beach ridges formed on the strandplains show an excellent record of lake-level changes. They are formed directly at the shoreline and have a good preservation potential as long as the lake-level declines. Satellite pictures of the northern strandplain show up to 230 beach ridges, but they are not equally well preserved at the different strandplain locations surrounding the lake. In this study, sediment from beach ridges were sampled for luminescence dating along two profiles (Figs. 1 and 2).

Profile 1 is located at the southeastern coast of Tangra Yum Co north-east of one of the large rivers flowing into the lake (Fig. 1). Directly north of the profile a smaller river incised into the strandplain (Fig. 2a). The main sediment influx comes from the major river in the south. The relief at this site is very low and beach ridges cover an area of up to ~70 m above the current lake level and a width of ~2.5 km. At higher elevations the beach ridges are replaced by strath terraces. Along this section beach-ridge sediments were sampled by excavating a hole in the uppermost part of the ridge and sampling a horizon with sand sized materials which is suitable for luminescence dating. The samples were mostly taken ~20–25 cm under the modern surface (Table 1). The beach ridges displayed undisturbed layers of gravel-sized sediments in a matrix of coarse to medium-sized sand and just small amounts of fine sand (Fig. 2a). Along this profile six samples for luminescence dating were collected from six beach ridges (Table 1) be-ginning at the current lake shore and going up to 66 m above current lake level. At higher elevations the beach ridges are smaller and finally replaced by strath terraces.

Profile 2 is located at the northern shore of Tangra Yum Co (Fig. 1). The slope of profile 2 is steeper than at profile 1, but gentler than nearby the lake shore areas. To the west of the profile a large river flows into the
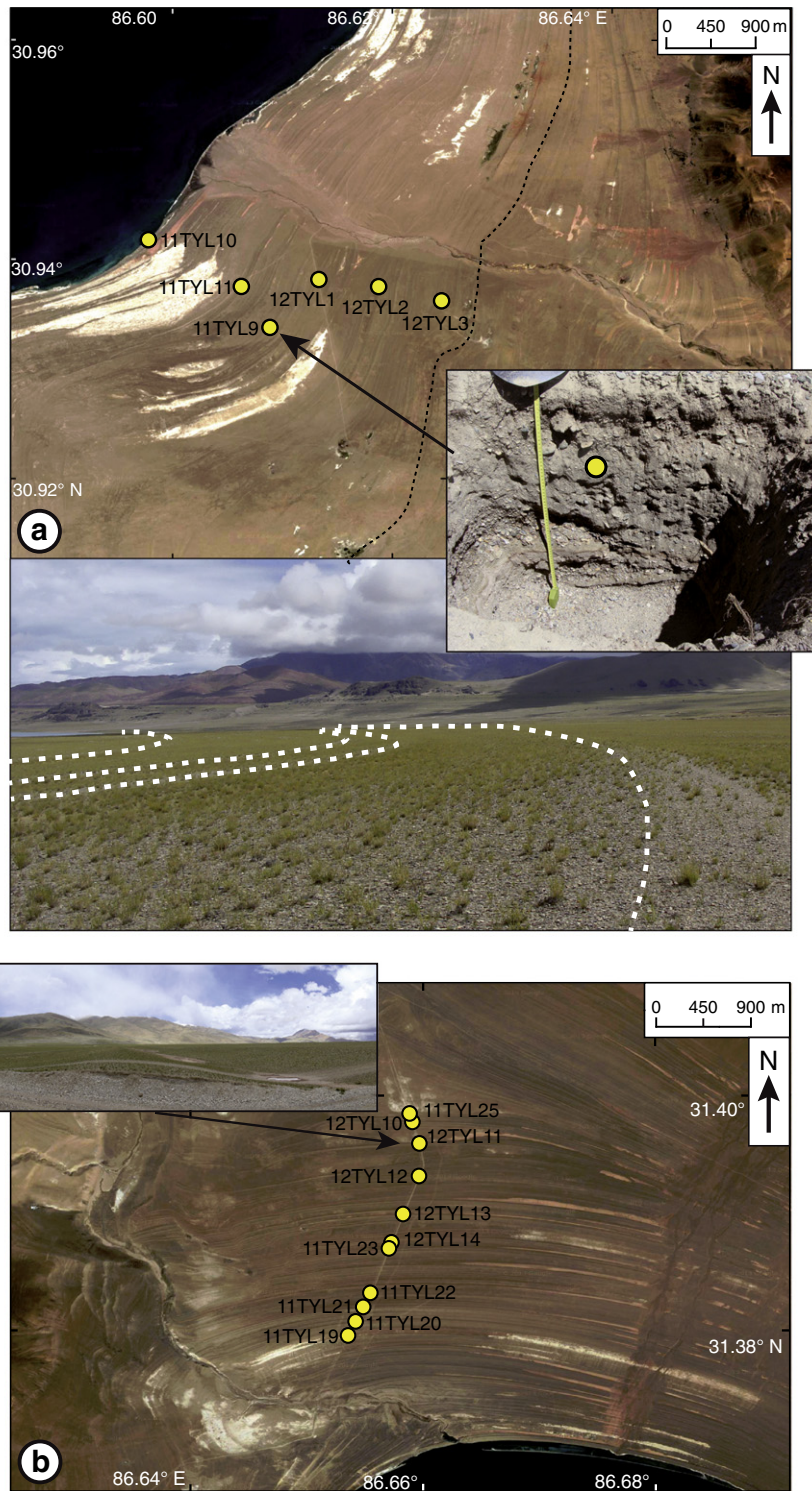
Figure 2. Satellite images of the two profiles giving an overview (exact location shown in Fig. 1b). The sampling locations are marked by yellow circles. (a) Satellite picture showing the sampling locations of profile 1. The strandplain increases in elevation towards the mountain face in a low angle. The black dashed line separates the strandplain from the terraces at this site. On the terraces no beach ridges were found. North of profile 1 a river is flowing into Tangra Yum Co, which is one of the sediment sources of the study area, but most of the sediments supposedly originates from the large river in the south (Fig. 1). The inset shows an example for sampling a beach ridge along profile 1. The photograph below shows a view over the beach ridges facing north. White, dashed lines mark the beach ridge crests. (b) The strandplain shows a steeper gradient than the one of profile 1. The beach ridges northeast of 11TYL25 have even higher elevations than 140 m above the lake level but the sediment was disturbed by animals and hence not suitable for luminescence dating.

lake, which incised very steeply into the sediments (Fig. 2b). The beach ridges of this strandplain extend from the current shoreline to elevations of more than 220 m. The sediments showed undisturbed layers of mostly gravel-sized sediments, in a matrix of coarse to medium-sized sand and small amounts of fine sand. The sand fraction is more abundant in these samples than at profile 1, but there is also a higher variability in the grain-size distribution among the beach ridges.

Table 1
Location of beach ridge samples at Tangra Yum Co and the grain size fraction used for luminescence dating.

Sample ID	Lum ID	Latitude WGS 84 (°N)	Longitude (°E)	Elevation of sample (m)	Elevation above lake level (m)	Depth below surface (m)	Grain size fraction (μm)
Profile 1 beach ridges southeast of Tangra Yumco							
11TYL10	2641	30.94180	86.59782	4545	0	0.25	250–300
11TYL11	2642	30.93753	86.60629	4560	15	0.20	250–300
11TYL9	2640	30.93380	86.60890	4574	29	0.60	250–300
12TYL1	2839	30.93817	86.61336	4581	36	0.20	250–300
12TYL2	2840	30.93752	86.61881	4598	53	0.20	250–300
12TYL3	2841	30.93622	86.62455	4611	66	0.20	150–250
Profile 2 beach ridges north of Tangra Yumco							
11TYL19	2650	31.37954	86.65355	4606	61	0.40	150–250
11TYL20	2651	31.38074	86.65420	4613	68	0.40	150–200
11TYL21	2652	31.38198	86.65486	4623	78	0.40	150–250
11TYL22	2653	31.38317	86.65547	4630	85	0.40	150–200
12TYL14	2852	31.38747	86.65729	4644	99	0.40	200–300
11TYL23	2654	31.38697	86.65706	4650	105	0.85	250–300
12TYL13	2851	31.38989	86.65828	4659	114	0.20	100–200
12TYL12	2850	31.39313	86.65966	4682	127	0.25	200–300
12TYL11	2849	31.39591	86.65969	4683	138	0.30	150–250
12TYL10	2848	31.39774	86.65908	4687	142	0.25	150–200
11TYL25	2656	31.39845	86.65885	4688	143	0.50	150–200

Along a road running north to south, eleven samples were taken from roadside outcrops 25–40 cm beneath the highest point of the beach ridge (Fig. 2b). Beach-ridge sediments were sampled from 61 m up to 143 m above lake level (Table 1). The sediments of beach ridges found at elevations higher than 143 m were affected by bioturbation and hence not suitable for luminescence dating.

Luminescence dating

Sample preparation

The samples for luminescence dating were processed following Aitken (1998). The sampled material was first dry sieved to extract a fraction of 150–200 μm. As in some cases the material from this fraction was too sparse the range of the fraction was extended up to 300 μm (Table 1). The samples were further treated with 10% HCL to remove carbonates and a 30% hydrogen peroxide solution was used to remove

the organic matter. Sodium oxalate was added to disperse possible aggregates. The K-feldspar rich fraction of minerals ρ < 2.58, as well as the quartz-rich fraction of 2.62 < ρ < 2.70, were then separated by density separation using sodium polytungstate solution. The quartz fraction was additionally etched using 40% hydrofluoric acid (HF) for 1 h, to remove the outer layer affected by α-radiation and dissolve possible feldspar contaminations. For the luminescence measurements the samples were mounted on stainless steel discs with silicon-oil spray using either the aliquot size of 6 mm containing ~1000 grains (Duller, 2008) or of 1 mm with ~10 grains.

Dose-rate determination

Samples for dose-rate determination were taken from the same layers as the luminescence samples. 700 g of dry sediment was homogenized and transferred to Marinelli beakers for gamma spectrometry measurement. Sample 12TYB10 was crushed in order to decrease the grain size. Afterwards all samples were stored for at least one month to assure equilibrium conditions for ^{226}Ra–^{222}Rn decay (Murray et al., 1987). The radioactivity of ^{40}K, U, Th and their daughter nuclides was measured using high-resolution gamma spectrometry with a high-purity germanium N-Type coaxial detector for at least 2 days (Table 2). The dose rates were calculated using the conversion factors given by Guérin et al. (2011), a-value was taken from Balescu et al. (2007) and beta-attenuation factors were chosen after Aitken (1985). We assumed a water content of 3 ± 1% because the beach ridges mostly consisted of coarser material and had no good water-holding capacity. Only for sample 11TYL10 the water content was measured (13%), because it was sampled at the lake shore and had higher water content than the other samples. Cosmic dose was calculated following Prescott and Stephan (1982) as well as Prescott and Hutton (1994).

Luminescence measurements

At first we tried to date the quartz fraction of the sampled sediments. Unexpectedly, we found anomalous fading rates of ~2–4%/decade in our quartz samples of both profiles (S. Tsukamoto and E. F. Rades, unpublished data). To our knowledge there are no studies regarding the applicability of fading correction to quartz. Therefore in this study we only use the K-feldspar fraction to set up a reliable chronological framework for the sediments of Tangra Yum Co, which has proven to yield reliable results compared to independent age control (Long et al., 2015).

Table 2
Radionuclide concentration (dry sediment), dose rate, residual doses, dose recovery test results and equivalent doses for all samples.

Sample ID	Radionuclide concentration			Cosmic dose rate (Gy/ka)	Total dose rate (Gy/ka)	Residual dose (IR$_{50}$) (Gy)	Residual dose (IRIR$_{170}$) (Gy)	Dose recovery (–)	Equivalent dose D$_e$ (IR$_{50}$) (Gy)	Equivalent dose D$_e$ (pIRIR$_{170}$) (Gy)
	U (ppm)	Th (ppm)	K (%)							
Profile 1 beach ridges southeast of Tangra Yumco										
11TYL10	3.05 ± 0.15	18.9 ± 1.0	2.90 ± 0.17	0.43 ± 0.04	5.46 ± 0.17	0.11 ± 0.02	0.22 ± 0.08	0.95 ± 0.04	0.20 ± 0.06	1.76 ± 0.65
11TYL11	2.99 ± 0.15	21.4 ± 1.1	2.89 ± 0.15	0.43 ± 0.04	6.08 ± 0.18	0.06 ± 0.04	0.11 ± 0.10	1.02 ± 0.01	2.68 ± 0.16	3.76 ± 0.28
11TYL9	3.53 ± 0.18	27.6 ± 1.4	3.18 ± 0.18	0.43 ± 0.04	6.86 ± 0.20	0.15 ± 0.01	0.35 ± 0.32	0.97 ± 0.25	5.64 ± 0.34	8.76 ± 0.55
12TYL1	2.96 ± 0.15	20.4 ± 1.0	2.17 ± 0.13	0.41 ± 0.04	5.24 ± 0.18	1.02 ± 0.39	1.03 ± 0.11	1.10 ± 0.04	48.7 ± 6.5	75.1 ± 4.0
12TYL2	4.51 ± 0.23	44.4 ± 2.2	3.96 ± 0.22	0.40 ± 0.04	8.92 ± 0.30	0.20 ± 0.02	0.86 ± 0.53	0.91 ± 0.15	22.1 ± 2.0	32.4 ± 4.7
12TYL3	5.04 ± 0.25	48.2 ± 2.4	4.08 ± 0.22	0.39 ± 0.04	9.40 ± 0.32	0.39 ± 0.32	0.39 ± 0.13	0.96 ± 0.08	12.2 ± 4.3	20.5 ± 5.3
Profile 2 beach ridges north of Tangra Yumco										
11TYL19	2.62 ± 0.13	12.37 ± 0.62	2.55 ± 0.14	0.44 ± 0.04	4.92 ± 0.23	0.11 ± 0.02	0.29 ± 0.04	1.12 ± 0.04	6.92 ± 0.19	8.76 ± 0.55
11TYL20	2.46 ± 0.12	11.38 ± 0.57	2.56 ± 0.15	0.44 ± 0.04	4.93 ± 0.17	0.11 ± 0.02	0.23 ± 0.03	1.13 ± 0.02	8.14 ± 0.19	9.91 ± 0.32
11TYL21	2.78 ± 0.14	10.79 ± 0.54	2.63 ± 0.15	0.44 ± 0.04	4.94 ± 0.23	0.11 ± 0.02	0.19 ± 0.01	1.17 ± 0.06	11.93 ± 0.34	13.88 ± 0.38
11TYL22	2.82 ± 0.14	11.70 ± 0.59	2.92 ± 0.17	0.44 ± 0.04	5.38 ± 0.18	0.07 ± 0.01	0.44 ± 0.03	1.06 ± 0.03	16.8 ± 1.6	21.4 ± 1.5
12TYL14	3.22 ± 0.16	9.09 ± 0.46	1.99 ± 0.11	0.37 ± 0.04	4.33 ± 0.16	0.32 ± 0.02	0.97 ± 0.20	0.91 ± 0.02	21.5 ± 1.5	33.4 ± 3.0
11TYL23	3.16 ± 0.16	9.16 ± 0.46	2.20 ± 0.12	0.44 ± 0.04	4.71 ± 0.15	0.12 ± 0.07	0.57 ± 0.41	1.11 ± 0.01	18.98 ± 0.49	26.2 ± 2.0
12TYL13	2.47 ± 0.12	8.87 ± 0.45	1.89 ± 0.10	0.36 ± 0.04	4.04 ± 0.15	0.19 ± 0.02	1.03 ± 0.04	0.93 ± 0.01	18.30 ± 0.44	33.2 ± 3.0
12TYL12	2.56 ± 0.13	8.50 ± 0.43	2.24 ± 0.12	0.35 ± 0.04	4.37 ± 0.16	0.25 ± 0.06	0.71 ± 0.08	0.93 ± 0.10	21.84 ± 0.42	29.6 ± 1.1
12TYL11	2.71 ± 0.14	10.44 ± 0.52	2.06 ± 0.11	0.35 ± 0.03	4.35 ± 0.15	0.25 ± 0.06	1.06 ± 0.08	1.05 ± 0.04	33.9 ± 4.1	60.7 ± 8.0
12TYL10	2.67 ± 0.13	10.64 ± 0.53	2.19 ± 0.12	0.34 ± 0.03	4.48 ± 0.16	0.12 ± 0.05	0.58 ± 0.22	1.13 ± 0.04	22.94 ± 0.87	27.99 ± 0.87
11TYL25	2.65 ± 0.13	10.19 ± 0.51	2.56 ± 0.14	0.44 ± 0.04	4.90 ± 0.17	0.20 ± 0.06	1.14 ± 0.14	1.39 ± 0.41	39.9 ± 1.4	49.7 ± 1.4

For all samples, except 11TYL10, a water content of 3% was assumed. The water content of 11TYL10, which was taken at the current shore was measured as 13%.

For the luminescence measurements an automated Risø TL/OSL DA-20 reader with an attached $^{90}Sr/^{90}Y$ beta source was used. Feldspar measurements were conducted using IR LEDs with a wavelength of 870 nm, using a Schott BG-39 filter as well as a neutral density filter of 10% from Lot Oriel because of the bright feldspar signal. For equivalent dose (D_e) measurements, each sample was measured using 10–12 large (6 mm) aliquots. For three samples (11TYL19, 12TYL3 and 12TYL13) the D_e values of 48 small aliquots containing ~10 grains were also measured for comparison. To minimise the effect of anomalous fading in the feldspar luminescence signal, the measurements were conducted using the post-IR infrared stimulated luminescence (pIRIR) protocol after Thomsen et al. (2008). Due to the expected young ages of the samples we applied a pIRIR protocol similar to Reimann et al. (2011) using a low preheat temperature at 200°C (60 s) and a post-IR stimulation at 170°C ($pIRIR_{170}$) for 300 s after bleaching with IR at 50°C (IR_{50}) for 100 s to reduce the residual dose (Table 3). As rejection criteria a recycling ratio limit of 10% difference from unity and a maximum test dose error of 10% were applied. The D_e values were calculated using the mean value of all aliquots and giving a 1σ standard error as uncertainty. The residual signal was measured for each sample using three aliquots bleached in a solar simulator (Hönle SOL2) for 4 h prior to measurement (Table 2). The intercept of the regression of the D_e against the residuals was calculated to 0.18 Gy (Fig. 3). Therefore the residual is negligibly low and no correction for the residual was applied to the natural D_e values. A dose recovery test was conducted for every sample using three aliquots with the same pretreatment as the aliquots for the residual test. After subtraction of the residual, dose recovery ratios were generally close to the unity (Table 2) except for sample 11TYL25, which was rejected because four of six aliquots gave ratios between 1.2 and 1.9. For sample 11TYL11 the dose recovery and residual were measured a second time, after 16 h bleaching in the solar simulator and the differences between both measurements were negligible.

The fading rates of the feldspar were determined following Auclair (2003) measuring a given dose of 44 Gy with time delays ranging from 0.1 to 45 h using the pIRIR protocol. The fading rates of the IR_{50} measurements are between ~4 to ~9%/decade (Table 4) while the fading rates for $pIRIR_{170}$ signals are less than ~2%/decade and thus regarded as negligible (Table 4, Fig. 4) (Buylaert et al., 2012). Thus the $pIRIR_{170}$ protocol successfully minimised the effects of anomalous fading for our samples. It should be noted that the fading rates for IR_{50} at profile 1 are much higher (~9%/decade) than the fading rates at profile 2 (~4 to ~7%/decade), which possibly reflects a difference in the source rocks.

Incomplete bleaching

Sediments, which undergo fluvial or wave transport, might be affected by incomplete bleaching. In addition the pIRIR signal, which is measured at an elevated temperature, is known to be harder to bleach than the quartz OSL and low temperature IRSL signals (Buylaert et al., 2012). The samples 12TYL1, 12TYL3 and 12TYL11 show large scatter in their D_e values (Figs. 5 and 6), which could be indicative for
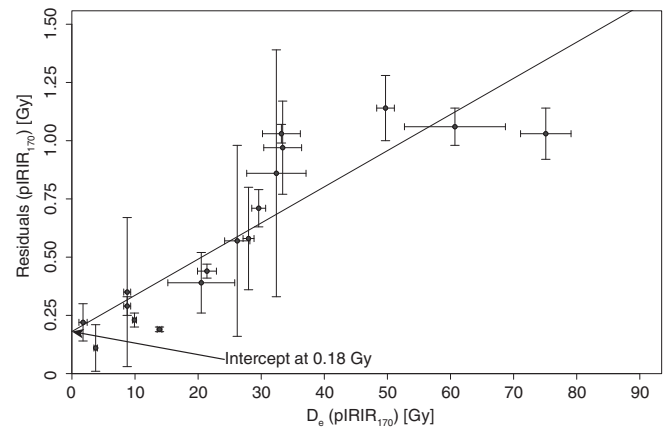

Figure 3. Scatter plot of D_e against the residual of each sample. A linear regression of the data shows an intercept with the y-axis of 0.18 Gy, which is negligible.

incomplete bleaching. In order to detect samples which have not been exposed to enough sunlight during their transport a comparison between the IR_{50} and $pIRIR_{170}$ D_e values was carried out following Buylaert et al. (2013). The IR_{50} bleaches much faster than the pIRIR signal (Buylaert et al., 2012). Therefore the ratio of IR_{50} and $pIRIR_{170}$ D_e values should be constant if the samples are well bleached and the fading rates are relatively uniform. Following Buylaert et al. (2013) we fitted our IR_{50} and $pIRIR_{170}$ D_e plot with a nonlinear equation $f_{(x)} = a(1-exp(-bx))$ (Fig. 6), except for the samples previously identified as poorly bleached (12TYL1, 12TYL3 and 12TYL11). The D_e value of 12TYL13 is plotted outside the 10% limit. This indicates that this sample is poorly bleached and therefore rejected. All the other samples are judged to be well bleached.

The regression curve fits to the data of both profiles despite the differences in g-values. Although there is a clear difference in the mean fading rates for the samples from the two sections, the slopes of the D_e plot of the sections cannot be distinguished by their positions in the scatter plot. Because of the young ages of the beach ridges we also tried to calculate a linear regression for the D_e values. As expected from the low D_e values of this section of the exponential function, the linear regression has nearly the same trend as the exponential function (data not shown).

To ensure that the scatter of the 6 mm aliquots and the comparison between IR_{50} and $pIRIR_{170}$ data really could be used as indicators for incomplete bleaching we also tested three samples using 48 aliquots with the size of 1 mm, reducing the amounts of measured grains to only ~10 grains. Our results for the well bleached sample 11TYL19 a higher over-dispersion and a bigger scatter using the smaller aliquots, but the mean D_e value is nearly the same (Figs. 5, 6). Sample 12TYL3 which already shows a large scatter using the 6 mm aliquots show an even higher over-dispersion for the 1 mm aliquots and showed a shift in the central age model D_e towards a smaller value (Figs. 5, 6). For sample 12TYL13 which showed no large scatter and was only identified as poorly bleached by the comparison between IR_{50} and $pIRIR_{170}$ the scatter increased largely (Figs. 5, 6), showing that the narrow distribution was caused by the averaging effect of the larger numbers of grains in the 6 mm aliquots.

Discussion

The samples acquired from two different profiles at Tangra Yum Co yielded a chronologically consistent succession of beach ridges. Most of the samples have been bleached sufficiently. This indicates that sediment movement took place near to the water surface over a sufficiently long period of time. In August 2012 we observed that most of the sediment at the shore is laterally transported along the shore and thus resulting in well bleached sediments. Four samples had to be rejected

Table 3
Protocol used to measure IR_{50} (steps 3 and 7) and $pIRIR_{170}$ (steps 4 and 8).

Step	Treatment	Observed
1	Give dose	
2	Preheat 200°C for 60 s	
3	Stimulation with IR for 100 s at 50°C	L_X ($IRSL_{50}$)
4	Stimulate with IR for 300 s at 170°C	L_X ($pIRIR_{170}$)
5[*]	Give test dose	
6	Preheat 200°C for 60 s	
7	Stimulation with IR for 100 s at 50°C	T_X ($IRSL_{50}$)
8	Stimulate with IR for 300 s at 170°C	T_X ($pIRIR_{170}$)

[*] Test dose ranged between 2 and 11 Gy depending on the expected natural signal of each sample.

Table 4
Fading rates and luminescence ages for all beach ridge samples taken at Tangra Yum Co, southern Tibet.

Sample ID	Elevation above lake level (m)	g-Value IR$_{50}$ (%/decade)	g-Value pIRIR$_{170}$ (%/decade)	Total dose rate (Gy/ka)	Age IR$_{50}$ (ka)	Age (fading corrected) IR$_{50}$* (ka)	Age pIRIR$_{170}$ (ka)
Profile 1 beach ridges southeast of Tangra Yumco							
11TYL10	0	8.91 ± 0.70	1.30 ± 0.24	5.46 ± 0.17	0.04 ± 0.01	–	0.32 ± 0.12
11TYL11	15	9.28 ± 0.55	0.96 ± 0.12	6.08 ± 0.18	0.44 ± 0.03	–	0.62 ± 0.05
11TYL9	29	8.10 ± 1.35	1.80 ± 0.34	6.86 ± 0.20	0.83 ± 0.05	–	1.28 ± 0.09
12TYL1	36	6.41 ± 0.43	1.70 ± 0.13	5.24 ± 0.18	9.42 ± 1.3	21.2 ± 4.4	14.4 ± 0.9
12TYL2	53	8.56 ± 0.80	1.75 ± 0.19	8.92 ± 0.30	2.50 ± 0.23	–	3.67 ± 0.54
12TYL3	66	8.45 ± 0.99	1.70 ± 0.30	9.40 ± 0.32	1.31 ± 0.46	–	2.21 ± 0.57
Profile 2 beach ridges north of Tangra Yumco							
11TYL19	61	5.77 ± 0.54	0.71 ± 0.09	4.92 ± 0.23	1.41 ± 0.08	2.71 ± 0.34	1.79 ± 0.14
11TYL20	68	4.34 ± 0.72	1.10 ± 0.50	4.93 ± 0.17	1.66 ± 0.07	2.58 ± 0.30	2.02 ± 0.09
11TYL21	78	3.85 ± 0.40	0.72 ± 0.08	4.94 ± 0.23	2.43 ± 0.13	3.55 ± 0.27	2.83 ± 0.15
11TYL22	85	3.63 ± 0.13	0.92 ± 0.09	5.38 ± 0.18	3.14 ± 0.31	4.52 ± 0.45	3.99 ± 0.31
12TYL14	99	4.74 ± 0.54	0.47 ± 0.35	4.33 ± 0.16	4.99 ± 0.39	8.55 ± 1.05	7.77 ± 0.74
11TYL23	105	3.51 ± 0.24	0.72 ± 0.20	4.71 ± 0.15	4.05 ± 0.17	5.76 ± 0.37	5.58 ± 0.46
12TYL13	114	4.46 ± 0.41	0.35 ± 0.34	4.04 ± 0.15	4.53 ± 0.20	7.43 ± 0.55	8.25 ± 0.80
12TYL12	127	3.82 ± 0.22	0.43 ± 0.16	4.37 ± 0.16	5.03 ± 0.20	7.46 ± 0.40	6.82 ± 0.34
12TYL11	138	4.18 ± 0.19	0.77 ± 0.29	4.35 ± 0.15	7.83 ± 0.98	12.4 ± 1.6	14.04 ± 1.9
12TYL10	142	3.96 ± 0.30	0.93 ± 0.14	4.48 ± 0.16	5.16 ± 0.26	7.88 ± 0.51	6.29 ± 0.29
11TYL25	143	7.17 ± 0.50	1.00 ± 0.15	4.90 ± 0.17	8.20 ± 0.39	24.0 ± 5.3	10.2 ± 0.5

* IR$_{50}$ ages corrected following Huntley and Lamothe (2001) using the Luminescence package for the statistics software R (Kreutzer et al., 2012). Fading correction for IR$_{50}$ ages could not be accomplished due to the young ages.

because of incomplete bleaching (12TYL1, 12TYL3 and 12TYL11) or because they did not pass the dose recovery test (11TYL25). Sample 12TYL13 showed only small scatter in the equivalent dose and was difficult to spot as not well bleached from its D$_e$ distribution. The sample taken at the shoreline (11TYL11) yields a depositional age of 300 a. Satellite pictures of the sampling site taken at different times show that the lake level rose by several metres from 2003 to 2009 (Wang et al., 2013). Therefore the "modern" sample perhaps gave the right age but the sediment sample was not taken from a beach ridge currently being formed. Generally, it is possible that some of the samples have been transported in just one storm event building the respective beach ridge. Therefore an inherited signal would be measured, because the sample has not been bleached at all during its last transportation process. This scenario would lead to even higher luminescence signal and therefore to a higher age. This is a conceivable scenario for samples 12TYL2 e.g. 12TYL4 which present themselves as outliers in the curve of lake-level decline (Fig. 7).

The data of this study indicates three distinct phases of lake-level decline since ~6.5 ka (Fig. 7). By regression analyses we estimated the rates of lake-level decline in these periods. Between ~6.5 and 4.5 ka the lake level declined with a rate of ~18 m/ka. Between 4.5 and 2 ka the fall of the lake level slowed down significantly to a rate of ~10 m/ka. Since ~2 ka the lake level dropped to its current elevation

with a rate of ~36 m/ka. The data of this study suggests a continuous decline of the lake level since 6.5 ka until at least ~300 a yr ago (Fig. 7). This is not necessarily the case, because a rising lake level would have eroded the beach ridges up to its highest point. However, events of this kind would show in the data by periods of no data. If lake level rises occurred since 6.5 ka they have most likely been short-term events.

Comparison with other lake-level histories on the Tibetan Plateau

Radiocarbon ages from lake sediments of the Tibetan Plateau have been obtained from bulk carbon samples or from organisms living in the lake. These samples are most often influenced by the reservoir effect which can be variable in time and account for errors of several thousand years (Hou et al., 2012). Luminescence dating is a good alternative to ^{14}C dating and has already been used on lacustrine and beach sediments on the Tibetan Plateau (Schütt et al., 2008; Li et al., 2009; Long et al., 2011).

Li et al. (2009) applied luminescence dating using a simplified multiple aliquot regenerative-dose (SMAR) protocol on polymineral fine-grained samples from beach ridges of Selin Co. Selin Co is located ~230 km northeast of Tangra Yum Co (Fig. 1). They sampled beach ridges up to 100 m above the current lake level of Selin Co. The highest beach ridges of Selin Co yielded ages of 67.9 ± 2.4 ka (101 m above the
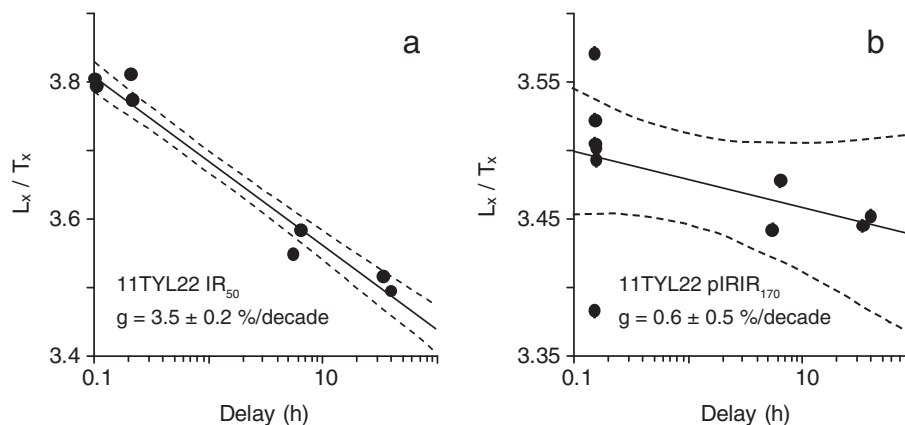

Figure 4. Fading rate measurements using IR$_{50}$ and pIRIR$_{170}$ signals. The L$_x$/T$_x$ ratio plotted against the delay time on a logarithmic scale. The dashed lines show the 1σ error range. (a) The steep inclination of the regression shows a fading rate of 3.5 ± 0.2%/decade for the IR$_{50}$ measurement. (b) The same aliquot measured at 170°C after the IR$_{50}$ measurement show a slighter inclination and a fading rate of only 0.6 ± 0.5%/decade.
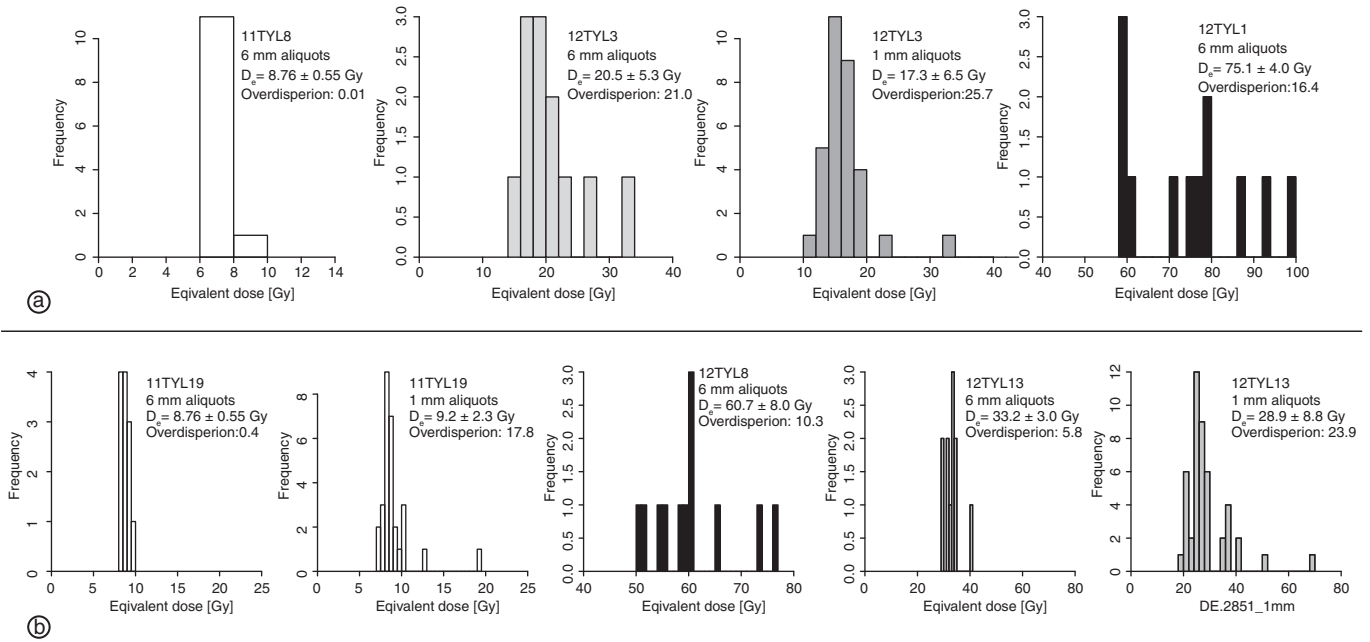
Figure 5. Histograms of the D_e distribution of six samples. (a) Four histograms showing the D_e distribution of samples from the southern profile 1. 11TYL8 is a sample classified as well bleached, whereas 12TYL1 and 12TYL3 show large scatter in their D_e values and are therefore considered as not well bleached. For sample 11TYL 3 a second measurement was conducted using 48 aliquots instead of only 12 and a smaller size of 1 mm confirming the high scatter of the obtained D_e values (b) All three shown here were sampled at the northern profile 2. Judging from the D_e distribution of the 6 mm aliquots samples 11TYL19 and 12TYL13 were classified as well bleached, whereas sample 12TYL11 shows large scatter and is considered as not well bleached. The comparison of IR_{50} and $pIRIR_{170}$ data showed that sample 12TYL13 is only partially bleached which can be confirmed by the scatter in the 48 1 mm aliquot measurements. The same measurement of sample 11TYL19 which showed no sign of being badly bleached confirmed the results from the 6 mm aliquot measurement.

lake), whereas in this study all beach ridges yielded Holocene ages. The data set of Li et al. (2009) shows significant age inversions with height, which compromise the reliability of the individual ages. Using the SMAR

protocol Li et al. (2009) only used 20 aliquots per sample from which 10–12 were used for D_e estimation and 6–8 for growth curve estimation, which contradicts the advantage of this method of measuring many natural signals very fast to get reliable results. Crucial for this method is the establishing of a reliable growth curve. Unfortunately characteristics for the growth curve quality are missing in the paper. The authors divided the sampled beach ridges into four groups, each representing a different climatic stage. The Holocene lake-level fluctuation of Selin Co seems to be restricted to 40 m (at 9.6 ± 0.7 ka) above
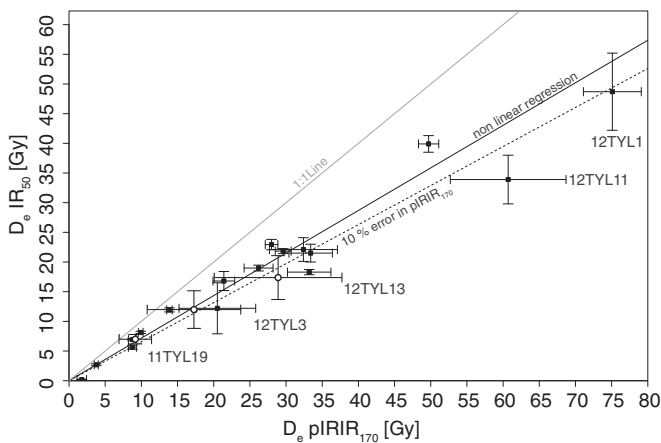

Figure 6. The average measured IR_{50} D_e values are plotted against the $pIRIR_{170}$ D_e values of the same measurement following Buylaert et al. (2013). Measurements done with 6 mm aliquots are shown as black rectangles and measurements using 1 mm aliquots as black circles. The error bars give the 1σ error. Due to anomalous fading present in the IR_{50} D_e values the data does not plot on a 1:1 line (grey solid line). The best fit for an exponential regression following the equation $f_{(x)} = a(1-exp(-bx))$ was calculated (solid black line). Another regression was calculated using the $pIRIR_{170}$ data multiplied by 1.1, showing the 10% error range (dashed black line). The samples 12TYL1, 12TYL3 and 12TYL11 show a big scatter in the D_e values, which is a good indicator for insufficient bleaching (Fig. 5). The large scatter can also be seen in the difference to the error bars of the other samples. Sample 12TYL13 which showed no such indication in the 6 mm aliquot measurement is more than 10% away from the solid line and not within one standard deviation. Therefore the sample was also rejected. For all other samples the signal has been zeroed prior to deposition. The same sample measured with 1 mm aliquots shows large scatter, which is again visible in the larger error bars. At the same time sample 11TYL19 which showed no indication to be badly bleached in the 6 mm aliquot measurement also classifies as well bleached using the 1 mm aliquots. This confirms that the rejection of the 6 mm aliquot measurement was correct and that this method to discriminate well and badly bleached samples works.
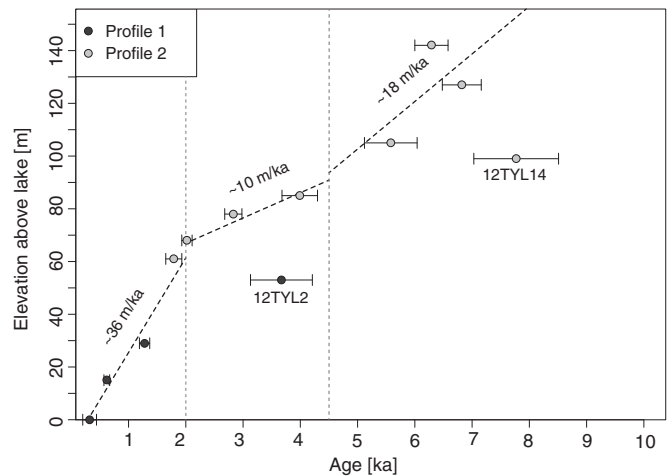

Figure 7. Elevation above the lake is plotted against the age derived from the $pIRIR_{170}$ measurements. Error bars are 1σ. The dated beach ridges are direct markers for the lake level and therefore the graph shows a lake-level chronology. Three distinct phases of lake-level decline can be seen between ~6.5 and 4.5 ka the lake level declined with a rate of ~18 m/ka. In the second period between 4.5 and 2 ka the rate of the lake-level decline was ~10 m/ka. During the last 2 ka the fastest decline can be observed with ~36 m/ka. The lake-level decline rates were calculated by linear regressions. Samples 12TYL2 and 12TYL14 were not considered for the calculation. The regression ~6.5 and 4.5 ka seems not to be very reliable and is probably higher.

the current lake level. In this time period Li et al. (2009) made out two groups of beach ridges. The two groups where classified as "Hypsithermal" and "Deglaciation" with ages ranging from 12.5 ± 1.6 ka to 1.9 ± 0.3 ka (Fig. 8). This implies rather small variations for the lake level of Selin Co during the Holocene compared to the data presented in our study while both lakes are located on the same latitude. However, the current lake area of Selin Co with >1830 km^2 is more than two times as big as todays lake area of Tangra Yum Co with 835 km^2 (Shao et al., 2008). This could be a possible reason for the difference in lake-level variations. Another possibility could be that the lakes were exposed to different climatic conditions before their Holocene highstand (Hudson and Quade, 2013).

Lee et al. (2009) studied beach ridges at Lagkor Tso ~260 km east of Tangra Yum Co (Fig. 1). They took four samples of beach ridges at 74 m, 105 m, 127 m and 130 m above the current lake. The samples were measured using optically stimulated luminescence (OSL) on quartz grains, yielding Holocene ages of 3.2 ± 0.8 ka, 3.7 ± 0.8 ka, 4.9 ± 0.2 ka, 5.2 ± 0.4 ka, respectively. The OSL ages are in the same age range as our results from Tangra Yum Co indicating a similar history for the Holocene lake-level decline (Fig. 8). However, a direct comparison between the Tangra Yum Co record and the OSL samples from Lagkor Tso remains difficult, because only four samples from paleoshorelines were taken by Lee et al. (2009), not yielding a whole chronology for the lake level.

At Zhari Namco, which is located directly west of Tangra Yum Co (Fig. 1), Chen et al. (2013) dated sediment samples from beach ridges. This lake is especially interesting because it has a similar lake area (996 km^2) as Tangra Yum Co (835 km^2; Shao et al. (2008)) but a different shape. Chen et al. (2013) took 22 samples from eleven shorelines to date the quartz with OSL dating. Eighteen samples were found to yield reliable ages of eight shorelines and the replica samples of the particular

shorelines yield consistent ages. According to Chen et al. (2013) the lake level dropped by 128 m over a period of 8.16 ± 0.46 ka (Fig. 8). The Holocene lake-level highstand of Zhari Namco at 128 m (Chen et al., 2013) is near to the 130–135 m of Tangra Yum Co as described by Rades et al. (2013). There is a hiatus in the chronology of Chen et al. (2013) during the period where our data shows a decreased rate for the lake-level fall (Fig. 8). Between ~2 and 1 ka the lake level of Zhari Namco seems to stay at the same level, but during this period our data shows the highest rate in lake-level decline for Tangra Yum Co. Overall the discrepancies between the data sets are quite small and fit well together.

Directly at the northwestern shore of Tangra Yum Co OSL dating of quartz from a deep lake sediment sequence of 200 cm thickness, located 25 m above the current lake level was carried out by Long et al. (2012) (Fig. 1). They dated the bottom of the sequence as 7.6 ± 0.6 ka and postulated a lake-level highstand to this time. The uppermost part of the sequence was dated to 2.7 ± 0.3 ka. Our luminescence dating indicates a lake level ~75 m higher than today at 2.7 ka. The uppermost 50 cm of the sequence dated by Long et al. (2012) were interpreted as shallow lake sediments. However, such a long period of shallow water should be visible as a plateau in the curve of lake-level decline, which cannot be seen in the data of our study (Fig. 7). In our quartz samples we found evidence of anomalous fading (S. Tsukamoto and E. F. Rades, unpublished data) which is a problem for dating. The samples used by Long et al. (2012) are from the same area as our samples. Therefore their samples may also have been affected by anomalous fading thus underestimated the true depositional age.

[10]Be exposure ages of strath terraces located ~140 m and ~180 m above the current lake level of Tangra Yum Co (Rades et al., 2013) are in relatively good agreement with the results of this study, if considering the entirely different methodological approaches. Still, there is an age
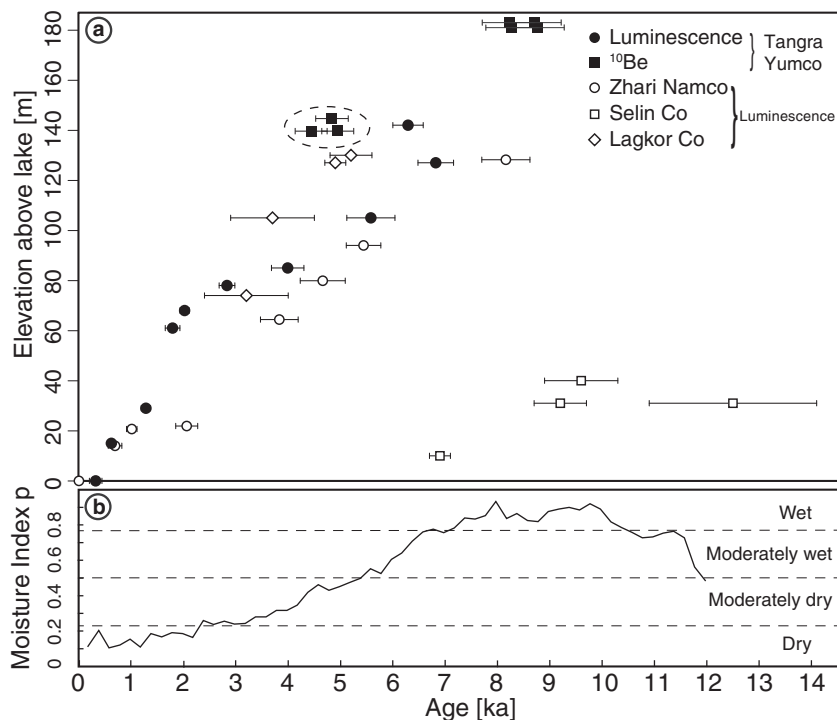

Figure 8. (a) Elevation above the lake plotted against the ages of the beach ridges. The data shown is taken from this study and the studies discussed in Lake level and monsoonal activity (Lee et al., 2009; Li et al., 2009; Chen et al., 2013; Rades et al., 2013). Note that the ages of the strath terraces from Rades et al. (2013) have been recalculated with the reassessed global production rate from Heyman (2014), but with otherwise unchanged parameters. Despite different lake sizes and shapes Tangra Yum Co, Lagkor Co and Zhari Namco had a very similar lake-level history throughout the Holocene. Selin Co, the easternmost lake, had smaller lake-level changes during the Holocene. The three samples encircled in with the dashed line are the ages of the lower terrace from the study of Rades et al. (2013) discussed in Comparison with other lake-level histories on the Tibetan Plateau. (b) Synthezied results of the Moisture index p in the monsoonal region of China after Zhang et al. (2011). The Moisture index shows that climate is getting drier since ~8 ka which corresponds to a lake-level decline in the same period shown by the luminescence and exposure ages in (a).

discrepancy of 1–2 ka between the ^{10}Be ages of ~4.0 to ~4.5 ka for the lower terrace and the luminescence ages for samples from beach ridges at a similar altitude (Fig. 8). This age discrepancy could, at least partly, be explained by an overestimation of the local ^{10}Be production rate employed by Rades et al. (2013), which was based on the global data set of Balco et al. (2008) and the time-dependent production rate scaling model of Lal (1991) and Stone (2000). Recently, a reassessment of the global ^{10}Be production rate data set was used to propose a production rate for the Tibetan Plateau that is ~12% lower (Heyman, 2014). This new production rate estimate would increase the ^{10}Be ages for the lower terrace by a similar amount (i.e. ~500 yr), which would distinctly decrease the gap between luminescence and ^{10}Be ages (Fig. 8). Likewise, the ^{10}Be ages of ~7.6 ka for the terrace ~180 m above the lake would be increased by about 900 yr. What is urgently required to reduce the uncertainty of exposure ages at the high altitudes of the Tibetan Plateau is a calibration site on the plateau, where local cosmogenic nuclide production rates can be reliably determined.

Lake level and monsoonal activity

Tangra Yum Co is located in a closed basin. The water balance of the lake depends on several factors. Often melting glaciers are perceived as cause for the high lake levels of closed lakes on the Tibetan Plateau (Wang et al., 2002; Kong et al., 2007). Many of the valleys surrounding Tangra Yum Co house glaciers or at least signs of former glacial activity. However, Hughes et al. (2013) suggested that in Tibet many glaciers did not advance or retreat at all during the Holocene or the time immediately preceding it. Although for some lakes glaciers may have been the main source of water during the past the potential ice volume surrounding Tangra Yum Co seems to be too small to account for the required influx to affect the water balance of the lake significantly. Tangra Yum Co is situated in an area affected by the Indian Summer Monsoon (ISM) (Zhang et al., 2011). The latter compiled the data of several oxygen isotope records from carbonates at ten lakes within the range of the ISM to generate an integrated Moisture index and combined them with oxygen isotope records from speleothems and carbon-isotope records from peat. The chronological framework used for this study is mainly based on ^{14}C dating. The authors state that for some sites the chronological control is relatively poor. As mentioned earlier in this section radiocarbon ages should be used with caution. However, in their synthesis the period with the highest humidity in Holocene was between 10.5 and 6.5 ka and since then a steady decrease in precipitation can be seen in their synthesized moisture indices, which corresponds to an arid phase between 4 to 0.5 ka from the study of Yu et al. (2013). This process matches our data of a steady lake-level decline shown by the pIRIR$_{170}$ ages of the beach ridges of Tangra Yum Co (Fig. 8). However, the lake-level decline is most probably not only a consequence of a lower precipitation, but an increase in solar insolation and therefore evaporation might also have had an influence (Dykoski et al., 2005). This study gives detailed information about the changes in lake level of Tangra Yum Co and improves the understanding of environmental change on the Tibetan Plateau throughout the Holocene.

Conclusions

A chronology for a lake-level decline of ~140 m has been established using the beach ridge successions on the northern and southeastern shores of Tangra Yum Co. The results indicate that the lake level has steadily declined during the past ~6.4 ka. For most of the 17 samples the feldspar material proved to be completely bleached during transport along the lake shore. By using the pIRIR$_{170}$ protocol on feldspar samples it was possible to minimise the problem of anomalous fading and determine reliable ages for the beach ridge successions under study. The measured IR$_{50}$ fading rates were high and differed significantly. By using a low preheat temperature of 200°C and a low measuring temperature of 170°C the residual levels have been minimised.

Our lake-level chronology based on feldspar luminescence dating at Tangra Yum Co is in good agreement with other studies using OSL or ^{10}Be surface exposure dating, which constrain former lake levels on the Tibetan Plateau. The cause of the lake-level decline is likely to be a lower precipitation rate since the early Holocene due to a weakened monsoonal activity since that time. Influences from tectonic activity or glacial melting seem to be negligible for this period.

References

Aitken, M.J., 1985. Thermoluminescence Dating. Academic Press, London.
Aitken, M.J., 1998. An Introduction to Optical Dating. Oxford University Press, Oxford.
Anthony, E.J., 1995. Beach-ridge development and sediment supply: examples from West Africa. Marine Geology 129, 175–186.
Auclair, M., 2003. Measurement of anomalous fading for feldspar IRSL using SAR. Radiation Measurements 37, 487–492.
Balco, G., Stone, J.O., Lifton, N.A., Dunai, T.J., 2008. A complete and easily accessible means of calculating surface exposure ages or erosion rates from ^{10}Be and ^{26}Al measurements. Quaternary Geochronology 3, 174–195.
Balescu, S., Ritz, J.-F., Lamothe, M., Auclair, M., Todbileg, M., 2007. Luminescence dating of a gigantic palaeolandslide in the Gobi-Altay mountains, Mongolia. Quaternary Geochronology 2, 290–295.
Buylaert, J.-P., Jain, M., Murray, A.S., Thomsen, K.J., Thiel, C., Sohbati, R., 2012. A robust feldspar luminescence dating method for Middle and Late Pleistocene sediments. Boreas 41, 435–451.
Buylaert, J., Murray, A.S., Gebhardt, A.C., Sohbati, R., Ohlendorf, C., Thiel, C., Wastegård, S., Zolitschka, B., 2013. Luminescence dating of the PASADO core 5022-1D from Laguna Potrok Aike (Argentina) using IRSL signals from feldspar. Quaternary Science Reviews 71, 70–80.
Chen, Y., Zong, Y., Li, B., Li, S., Aitchison, J.C., 2013. Shrinking lakes in Tibet linked to the weakening Asian monsoon in the past 8.2 ka. Quaternary Research 80, 189–198.
Daut, G., Mäusbacher, R., Baade, J., Gleixner, G., Kroemer, E., Mügler, I., Wallner, J., Wang, J., Zhu, L., 2010. Late Quaternary hydrological changes inferred from lake level fluctuations of Nam Co (Tibetan Plateau, China). Quaternary International 218, 86–93.
Doberschütz, S., Frenzel, P., Haberzettl, T., Kasper, T., Wang, J., Zhu, L., Daut, G., Schwalb, A., Mäusbacher, R., 2013. Monsoonal forcing of Holocene paleoenvironmental change on the central Tibetan Plateau inferred using a sediment record from Lake Nam Co (Xizang, China). Journal of Paleolimnology 51, 253–266.
Duller, G.A.T., 2008. Single-grain optical dating of Quaternary sediments: why aliquot size matters in luminescence dating. Boreas 37, 589–612. http://dx.doi.org/10.1111/j.1502-3885.2008.00051.x.
Dykoski, C.A., Edwards, L.R., Cheng, H., Yuan, D., Cai, Y., Zhang, M., Lin, Y., Qing, J., An, Z., Revenaugh, J., 2005. A high-resolution, absolute-dated Holocene and deglacial Asian monsoon record from Dongge Cave, China. Earth and Planetary Science Letters 233, 71–86.
Forsyth, A.J., Nott, J., Bateman, M.D., 2010. Beach ridge plain evidence of a variable late-Holocene tropical cyclone climate, North Queensland, Australia. Palaeogeography, Palaeoclimatology, Palaeoecology 297, 707–716.
Frenzel, P., Wrozyna, C., Xie, M., Zhu, L., Schwalb, A., 2010. Palaeo-water depth estimation for a 600-year record from Nam Co (Tibet) using an ostracod-based transfer function. Quaternary International 218, 157–165.
Gasse, F., Arnold, M., Fontes, J.C., Fort, M., Gibert, E., Huc, A., Bingyan, L., Yuanfang, L., Qing, L., Mélières, F., Van Campo, E., Fubao, W., Qinsong, Z., 1991. A 13,000-year climate record from western Tibet. Nature 353, 742–745.
Guérin, G., Mercier, N., Adamiec, G., 2011. Dose-rate conversion factors: update. Ancient TL 29, 5–8.
Harvey, N., 2006. Holocene coastal evolution: barriers, beach ridges, and tidal flats of South Australia. Journal of Coastal Research 221, 90–99.
Heyman, J., 2014. Paleoglaciation of the Tibetan Plateau and surrounding mountains based on exposure ages and ELA depression estimates. Quaternary Science Reviews 91, 30–41.
Hipondoka, M.H.T., Mauz, B., Kempf, J., Packman, S., Chiverrell, R.C., Bloemendal, J., 2014. Chronology of sand-ridges and the Late Quaternary evolution of the Etosha Pan, Namibia. Geomorphology 204, 553–563.
Hou, J., D'Andrea, W.J., Liu, Z., 2012. The influence of ^{14}C reservoir age on interpretation of paleolimnological records from the Tibetan Plateau. Quaternary Science Reviews 48, 67–79.
Hudson, A.M., Quade, J., 2013. Long-term east–west asymmetry in monsoon rainfall on the Tibetan Plateau. Geology 41, 351–354.

Hughes, P.D., Gibbard, P.L., Ehlers, J., 2013. Timing of glaciation during the last glacial cycle: evaluating the concept of a global "Last Glacial Maximum" (LGM). Earth-Science Reviews 125, 171–198.

Huntley, D.J., Lamothe, M., 2001. Ubiquity of anomalous fading in K-feldspars and the measurement and correction for it in optical dating. Canadian Journal of Earth Sciences 38, 1093–1106.

Jacobs, Z., 2008. Luminescence chronologies for coastal and marine sediments. Boreas 37, 508–535.

Kong, P., Na, C., Fink, D., Huang, F., Ding, L., 2007. Cosmogenic [10]Be inferred lake-level changes in Sumxi Co basin, Western Tibet. Journal of Asian Earth Sciences 29, 698–703.

Kreutzer, S., Schmidt, C., Fuchs, M.M.C., Dietze, M., Fischer, M., 2012. Introducing an R package for luminescence dating analysis. Ancient TL 30, 1–8.

Lai, Z.P., Mischke, S., Madsen, D., 2014. Paleoenvironmental implications of new OSL dates on the formation of the "Shell Bar" in the Qaidam Basin, northeastern Qinghai–Tibetan Plateau. Journal of Paleolimnology 51, 197–210.

Lal, D., 1991. Cosmic ray labeling of erosion surfaces: in situ nuclide production rates and erosion models. Earth and Planetary Science Letters 104, 424–439. http://dx.doi.org/10.1016/0012-821X(91)90220-C.

Lee, J., Li, S., Aitchison, J.C., 2009. OSL dating of paleoshorelines at Lagkor Tso, western Tibet. Quaternary Geochronology 4, 335–343.

Li, D., Li, Y., Ma, B., Dong, G., Wang, L., Zhao, J., 2009. Lake-level fluctuations since the Last Glaciation in Selin Co (lake), Central Tibet, investigated using optically stimulated luminescence dating of beach ridges. Environmental Research Letters 4, 045204 (10 pp.).

Liu, X., Lai, Z., Madsen, D., Yu, L., Liu, K., Zhang, J., 2011. Lake level variations of Qinghai Lake in northeastern Qinghai–Tibetan Plateau since 3.7 ka based on OSL dating. Quaternary International 236, 57–64.

Liu, X.-J., Lai, Z.-P., Zeng, F.-M., Madsen, D.B., E., C.-Y., 2013. Holocene lake level variations on the Qinghai–Tibetan Plateau. International Journal of Earth Sciences 102, 2007–2016.

Long, H., Lai, Z., Wang, N., Zhang, J., 2011. A combined luminescence and radiocarbon dating study of Holocene lacustrine sediments from arid northern China. Quaternary Geochronology 6, 1–9.

Long, H., Lai, Z., Frenzel, P., Fuchs, M., Haberzettl, T., 2012. Holocene moist period recorded by the chronostratigraphy of a lake sedimentary sequence from Lake Tangra Yumco on the south Tibetan Plateau. Quaternary Geochronology 10, 136–142.

Long, H., Haberzettl, T., Tsukamoto, S., Shen, J., Kasper, T., Daut, G., Zhu, L., Mäusbacher, R., Frechen, M., 2015. Luminescence dating of lacustrine sediments from Tangra Yumco (southern Tibetan Plateau) using post-IR IRSL signals from polymineral grains. Boreas 44, 139–152. http://dx.doi.org/10.1111/bor.12096.

Ma, R., Yang, G., Duan, H., Jiang, J., Wang, S., Feng, X., Li, A., Kong, F., Xue, B., Wu, J., Li, S., 2011. China's lakes at present: number, area and spatial distribution. Science China Earth Sciences 54, 283–289.

Mischke, S., Aichner, B., Diekmann, B., Herzschuh, U., Plessen, B., Wünnemann, B., Zhang, C., 2010. Ostracods and stable isotopes of a late glacial and Holocene lake record from the NE Tibetan Plateau. Chemical Geology 276, 95–103.

Morrill, C., Overpeck, J.T., Cole, J.E., Liu, K., 2006. Holocene variations in the Asian monsoon inferred from the geochemistry of lake sediments in central Tibet. Quaternary Research 65, 232–243.

Murray, A.S., Marten, R., Johnston, A., Martin, P., 1987. Analysis for naturally occuring radionuclides at environmental concentrations by gamma spectrometry. Journal of Radioanalytical and Nuclear Chemistry 115, 263–288.

Nielsen, A., Murray, A.S., Pejrup, M., Elberling, B., 2006. Optically stimulated luminescence dating of a Holocene beach ridge plain in Northern Jutland, Denmark. Quaternary Geochronology 1, 305–312.

Opitz, S., Wünnemann, B., Aichner, B., Dietze, E., Hartmann, K., Herzschuh, U., IJmker, J., Lehmkuhl, F., Li, S., Mischke, S., Plotzki, A., Stauch, G., Diekmann, B., 2012. Late Glacial and Holocene development of Lake Donggi Cona, north-eastern Tibetan Plateau, inferred from sedimentological analysis. Palaeogeography, Palaeoclimatology, Palaeoecology 337–338, 159–176.

Ortlieb, L., Fournier, M., Macharé, J., 1992. Sequences of Holocene beach ridges in northern Peru–chronological framework and possible relationships with former El Niño events. Paleo ENSO Records International Symposium, Lima March 1992, pp. 215–224.

Otvos, E.G., 2000. Beach ridges — definitions and significance. Geomorphology 32, 83–108.

Prescott, J.R., Hutton, J.T., 1994. Cosmic ray contributions to dose rates for luminescence and ESR dating: large depths and long-term time variations. Radiation Measurements 23, 497–500.

Prescott, J.R., Stephan, L.G., 1982. The contribution of cosmic radiation to the environmental dose for thermoluminescent dating latitude, altitude and depth dependences. PACT 6, 17–25.

Rades, E.F., Hetzel, R., Xu, Q., Ding, L., 2013. Constraining Holocene lake-level highstands on the Tibetan Plateau by [10]Be exposure dating: a case study at Tangra Yumco, southern Tibet. Quaternary Science Reviews 82, 68–77.

Reimann, T., Tsukamoto, S., Harff, J., Osadczuk, K., Frechen, M., 2011. Reconstruction of Holocene coastal foredune progradation using luminescence dating — an example from the Świna barrier (southern Baltic Sea, NW Poland). Geomorphology 132, 1–16.

Schütt, B., Berking, J., Frechen, M., Yi, C., 2008. Late Pleistocene lake level fluctuations of the Nam Co, Tibetan Plateau, China. Zeitschrift für Geomorphologie, Supplementary Issues 52, 57–75.

Shao, Z., Meng, X., Zhu, D., Zheng, D., Qiao, Z., Yang, C., Han, J., Yu, J., Meng, Q., Lü, R., 2008. Characteristics of the change of major lakes on the Qinghai–Tibet Plateau in the last 25 years. Frontiers of Earth Science in China 2, 364–377.

Stone, J.O., 2000. Air pressure and cosmogenic isotope production. Journal of Geophysical Research 105, 23753. http://dx.doi.org/10.1029/2000JB900181.

Sun, Y., Lai, Z., Long, H., Liu, X., Fan, Q., 2010. Quartz OSL dating of archaeological sites in Xiao Qaidam Lake of the NE Qinghai–Tibetan Plateau and its implications for palaeoenvironmental changes. Quaternary Geochronology 5, 360–364. http://dx.doi.org/10.1016/j.quageo.2009.02.013.

Tamura, T., Saito, Y., Bateman, M.D., Nguyen, V.L., Ta, T.K.O., Matsumoto, D., 2012. Luminescence dating of beach ridges for characterizing multi-decadal to centennial deltaic shoreline changes during Late Holocene, Mekong River delta. Marine Geology 326–328, 140–153.

Thomsen, K.J., Murray, A.S., Jain, M., Bøtter-Jensen, L., 2008. Laboratory fading rates of various luminescence signals from feldspar-rich sediment extracts. Radiation Measurements 43, 1474–1486.

Wang, R., Scarpitta, S., Zhang, S., Zheng, M., 2002. Later Pleistocene/Holocene climate conditions of Qinghai–Xizhang Plateau (Tibet) based on carbon and oxygen stable isotopes of Zabuye Lake sediments. Earth and Planetary Science Letters 203, 461–477.

Wang, X., Gong, P., Zhao, Y., Xu, Y., Cheng, X., Niu, Z., Luo, Z., Huang, H., Sun, F., Li, X., 2013. Water-level changes in China's large lakes determined from ICESat/GLAS data. Remote Sensing of Environment 132, 131–144.

Wei, K., Gasse, F., 1999. Oxygen isotopes in lacustrine carbonates of West China revisited: implications for post glacial changes in summer monsoon circulation. Quaternary Science Reviews 18, 1315–1334.

Yan, D., Wünnemann, B., 2014. Late Quaternary water depth changes in Hala Lake, northeastern Tibetan Plateau, derived from ostracod assemblages and sediment properties in multiple sediment records. Quaternary Science Reviews 95, 95–114.

Yu, L., Lai, Z., An, P., 2013. OSL chronology and paleoclimatic implications of paleodunes in the middle and southwestern Qaidam Basin, Qinghai–Tibetan Plateau. Sciences in Cold and Arid Regions 5 (2), 211–219. http://dx.doi.org/10.3724/SP.J.1226.2013.00211.

Zhang, J., Chen, F., Holmes, J.A., Li, H., Guo, X., Wang, J., Li, S., Lü, Y., Zhao, Y., Qiang, M., Lue, Y., 2011. Holocene monsoon climate documented by oxygen and carbon isotopes from lake sediments and peat bogs in China: a review and synthesis. Quaternary Science Reviews 30, 1973–1987.

Zhao, Y., Yu, Z., Zhao, W., 2011. Holocene vegetation and climate histories in the eastern Tibetan Plateau: controls by insolation-driven temperature or monsoon-derived precipitation changes? Quaternary Science Reviews 30, 1173–1184.